Low-Dimensional Semiconductor Superlattices Formed by Geometric Control over Nanocrystal Attachment: Supporting Information for the Theoretical Study

W. H. Evers,[1] B. Goris,[2] S. Bals,[2] M. Casavola,[1] J. de Graaf,[1] R. van Roij,[3] M. Dijkstra,[1] and D. Vanmaekelbergh[1,*]

[1] *Soft Condensed Matter, Debye Institute for Nanomaterials Science, Utrecht University, Princetonplein 1, 3584 CC Utrecht, The Netherlands*

[2] *EMAT, Dept. of Physics, University of Antwerpen, Groenenborgerlaan 171, 2010 Antwerpen, Belgium*

[3] *Institute for Theoretical Physics, Utrecht University, Leuvenlaan 4, 3584 CE Utrecht, The Netherlands*

(Dated: July 27, 2012)

INTERFACIAL ADSORPTION OF A TRUNCATED CUBE

In this section we consider the adsorption of a single truncated (nano)cube at a flat toluene-air interface using a theoretical model based on surface-tension arguments. We apply a model similar to that of P. Pieranski, who analysed the strength of adsorption of spherical colloids at liquid-gas and liquid-liquid interfaces [1].

The Model for the Truncated Cubes

To describe the experimental system, we consider a truncated cube which, in its initial configuration, is given by the set of vertices

$$\{\mathbf{v}(q)\} = \frac{\mathcal{P}_D\left((\pm 1, \pm(1-q), \pm(1-q))^T\right)}{\sqrt{4(\sqrt{3}q^2 + 6\sqrt{2}q(1-q) + 6(1-q)^2)}}, \tag{1}$$

where $q \in [0,1]$ is the truncation parameter, 'T' indicates transposition, $\mathcal{P}_D$ is a permutation operation that generates all permutations of each element in the set of 8 vertices spanned by the $\pm$-operations (which are allowed to act independently of each other). By letting $\mathcal{P}_D$ act we obtain 48 vertices. Subsequent deletion of all duplicates reduces this set to the desired total of 24 vertices for a truncated cube with 6 {100}, 12 {110}, and 8 {111} facets. The expression in the denominator ensures that the truncated cube is normalized to unit surface area. By changing the value of q the truncated cube deforms smoothly from a cube ($q = 0$) to an octahedron ($q = 1$) *via* a cuboctahedron ($q = \sqrt{2}/(\sqrt{2}+1) \approx 0.586$), also see Fig. 1a, which shows our model for various levels of truncation. We restrict ourselves to $q \in [0, 0.6]$ in the following.

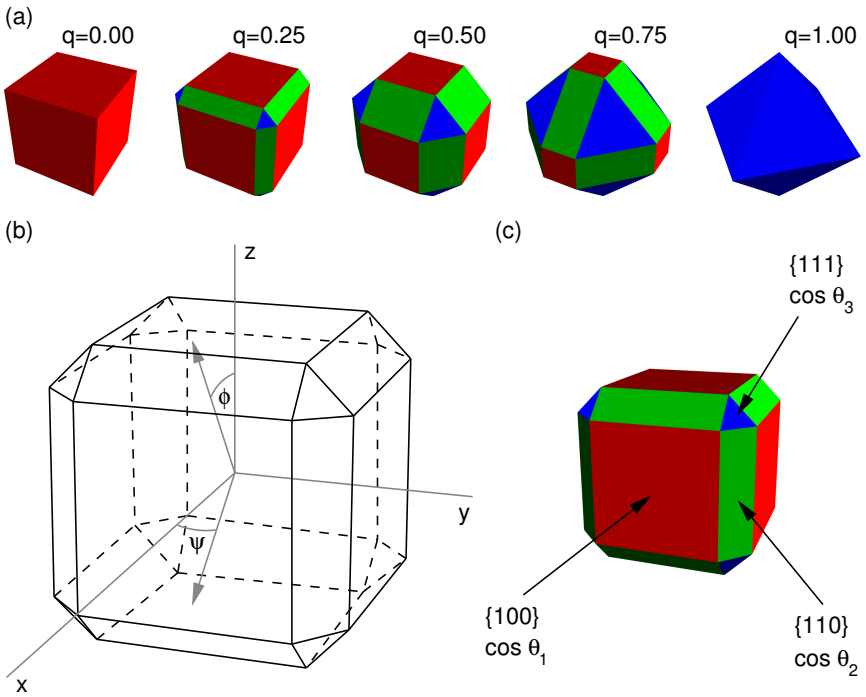

FIG. 1. (a) The truncated cube model for several values of the truncation parameter $q \in [0,1]$. (b) A schematic representation of the model for $q = 0.30$ which shows the truncated cube in its initial configuration, i.e., the normals of the {100} facets are axis-aligned and its centre coincides with the origin. We also indicated the azimuthal angle ψ and the polar angle ϕ. To keep the picture clear, we did not show the interface or the height z, which is zero in this case. (c) The three types of facets: (red) a {100} facet, (green) a {110} facet, and (blue) a {111} facet. The figure also shows the corresponding cosine of the contact angle $\cos\theta_i$, with $i = 1, 2, 3$, that is used to describe the surface properties of the respective facets.

In its initial configuration the truncated cube has the normals of its {100} facets aligned with the axes of a standard Cartesian coordinate frame and its centre coincides with the origin. When this truncated cube is brought into contact

with a flat *undeformed* liquid-gas or liquid-liquid interface, the system can be described by four parameters: (i) the size of the particle, which is given by the multiplicative factor s that acts on the vertices in Eq. (1); (ii) the height z of the particle with respect to the interface (as measured along the z-axis), which we locate at $z = 0$ (xy-plane); (iii) rotation by the azimuthal angle ψ (around the z-axis); and (iv) rotation by the polar angle ϕ (around the y-axis). The angles are indicated in Fig. 1b. We assume that the truncated cube is first scaled by s, then rotated by ψ and subsequently by ϕ, and finally it is translated by z. Due to the symmetry properties of the truncated cube we can restrict ourselves to $\psi \in [0, \pi/4]$ and $\phi \in [0, \pi/2]$. Even for this restricted range there are several instances of duplicate orientations, e.g., $\psi \in [0, \pi/4]$ and $\phi = 0$ gives essentially the same configuration as $\psi = 0$ and $\phi = \pi/2$. These duplicate configurations are taken into account via congruence in our analysis.

The Free Energy of Adsorption

In the experiments there is an indication that the surface properties of the different facets can vary with the particle concentration, see the main text. Effectively, the ligand covering of the various facets is influenced by the ligand concentration in the ethylene glycol via adsorption-desorption equilibria. To describe this in our model, we assume that the different crystal planes, i.e., the {100}, {110}, and {111} facets, have surface properties that can vary independently of each other, but are otherwise the same for facets of the same type. In this system the free energy of adsorption F can be written as

$$F(z, \psi, \phi) = \gamma_{12}(A - S_{12}) + \gamma_{1t}S_{1t} + \gamma_{1b}S_{1b} + \gamma_{2t}S_{2t} + \gamma_{2b}S_{2b} + \gamma_{3t}S_{3t} + \gamma_{3b}S_{3b}, \tag{2}$$

where γ_{12} is the liquid-air interfacial tension, A is the total surface area of the interface, S_{12} is the surface area excluded from the interface by the presence of the colloid, γ_{it} is the surface tension between facets of type i ($i = 1$, 2, 3) and the top medium, S_{it} is the total surface area of the facets of type i in contact with the top medium, γ_{ib} is the surface tension between facets of type i and the bottom medium, and S_{ib} is the total surface area of the facets of type i in contact with the bottom medium. Note that we have made the dependence of S_{12}, S_{it}, and S_{ib} on (z, ψ, ϕ) implicit. In this model the microscopic degrees of freedom of the solvent molecules were integrated out to give surface tensions. We further assumed that the interface is not deformed by the presence of the particle: capillary deformation by gravity, electrostatic effects, or contact-angle requirements. These are strong simplifications, but there are too many unknowns regarding the experimental system to justify a more extended model. In this light, the results obtained in the next section should be seen as an indication of the possible behaviour of a truncated cube at a liquid-air or liquid-liquid interface, rather than a full theoretical description of the phenomenology in the experimental system. We will come back to the quality of these results in the discussion.

To simplify the calculations we can reduce Eq. (2) by subtracting a constant contribution to the free energy of adsorption

$$\begin{aligned} F'(z, \psi, \phi) &= F(z, \psi, \phi) - [\gamma_{12}A + \gamma_{1b}(S_{1t} + S_{1b}) + \gamma_{2b}(S_{2t} + S_{2b}) + \gamma_{3b}(S_{3t} + S_{3b})]\,; & (3)\\ &= (\gamma_{1t} - \gamma_{1b})S_{1t} + (\gamma_{2t} - \gamma_{2b})S_{2t} + (\gamma_{3t} - \gamma_{3b})S_{3t} - \gamma_{12}S_{12}; & (4)\\ &= \gamma_{12}\left[\cos\theta_1 S_{1t} + \cos\theta_2 S_{2t} + \cos\theta_3 S_{3t} - S_{12}\right], & (5) \end{aligned}$$

where we set the shifted free energy F' to zero when the colloid is completely immersed in the bottom medium. In the last step [Eq. (5)] we used Young's equation [2]

$$\gamma_{it} = \gamma_{12}\cos\theta_i + \gamma_{ib}, \tag{6}$$

with θ_i the contact angle corresponding to the (type i facet - top medium - bottom medium) three-phase contact. Figure 1c shows the correspondence between the different contact angles and the various facets: the surface properties of the {100} facets are described by θ_1, those of {110} facets by θ_2, and those of the {111} facets by θ_3. Note that the θ_i are determined by material properties, whereas ψ and ϕ are variables in our theory. Using the above equations we can now write the dimensionless free energy of adsorption as

$$\begin{aligned} f(z, \psi, \phi) &\equiv \frac{F'(z, \psi, \phi)}{\gamma_{12}S}; & (7)\\ &= \cos\theta_1 r_{1t} + \cos\theta_2 r_{2t} + \cos\theta_3 r_{3t} - r_{12}, & (8) \end{aligned}$$

with $r_{it} \equiv S_{it}/S$ and $r_{12} \equiv S_{12}/S$. Note that the dependence of f on the level of truncation q and the surface properties and media (via the contact angles θ_i) is implicit in Eq. (7). Moreover, Eq. (7) is independent of the size s of the particle.

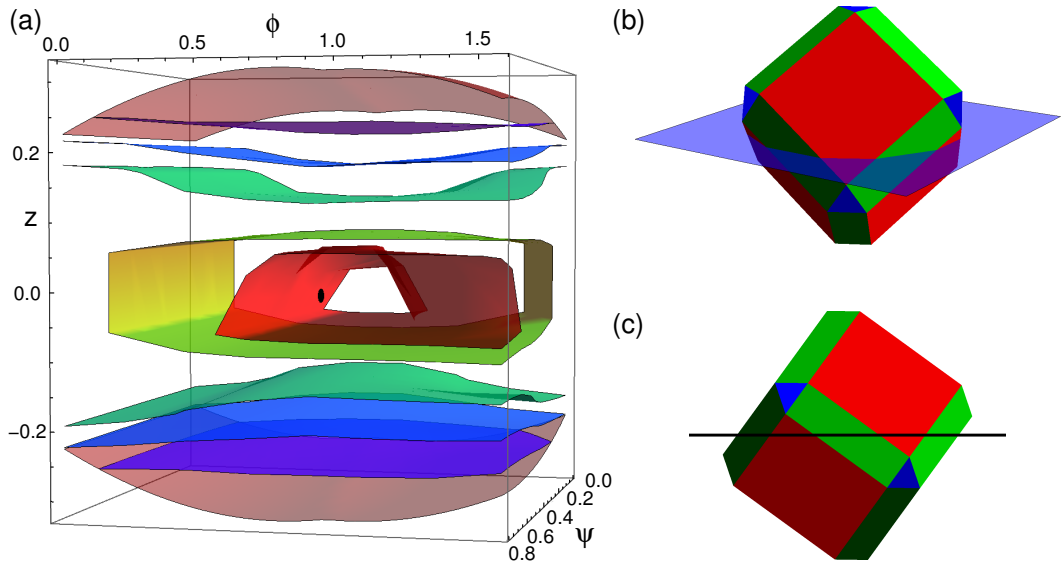

FIG. 2. The free energy of adsorption f for a truncated cube model with $q = 0.30$ and $\cos\theta_i = 0$, for $i = 1, 2, 3$. Note that this choice for the contact angles ensures that adsorption is completely determined by excluded surface area considerations, also see Eq. (7). (a) A contour plot of the three-dimensional (3D) free-energy landscape: f as a function of the adsorption depth z, the azimuthal angle ψ, and the polar angle ϕ. The top and bottom red surface indicate for which z value the truncated cube just touches the interface, for a given ψ and ϕ. From blue to red the contours give $f = -0.05$, -0.10, -0.15, -0.20, and -0.22. The location of the free-energy minimum is indicated using a black dot. For this particular system we find that $f(z, \psi, \phi)_{\min} \approx -0.24$ and that $(z, \psi, \phi)_{\min} \approx (0.00, 0.25\pi, 0.30\pi)$. (b) The truncated cube in its equilibrium position; one of the {111} facets is pointing in the direction of the z-axis. The translucent blue square indicates the interface. (c) A side view of the truncated cube in this equilibrium position, the thick black line indicates the interface.

For a given q, θ_1, θ_2, and θ_3, Eq. (7) gives rise to a three-dimensional (3D) free energy of adsorption landscape, see Fig. 2 for an example. This landscape was established by numerically determining the values of r_{1t}, r_{2t}, r_{3t}, and r_{12} on a (z, ψ, ϕ) grid, which can be easily accomplished using the triangular-tessellation technique described in Refs. [3, 4]. In the case of a faceted particle our technique's results are exact. The normalization in Eq. (1) allows us to directly obtain the fractional values r_{it} and r_{12}. In the following we take $z \in [-0.4, 0.4]$, $\psi \in [0, \pi/4]$, and $\phi \in [0, \pi/2]$ with 100 equidistant steps for each of these parameters. Whenever $s = 1$, the radius of a circumscribed sphere for our truncated cube is always smaller than 0.4. This implies that our choice of $z \in [-0.4, 0.4]$ always samples the full range of adsorption configurations.

The thermodynamic equilibrium is assumed in the minimum of the free-energy landscape, i.e., the z, ψ, and ϕ combination for which f has the lowest value; we will denote this minimum as $(z, \psi, \phi)_{\min}$. This point can be easily approximated by searching through our free-energy landscape on a grid for the (z, ψ, ϕ) combination that gives the lowest value of f. The density of grid points (100^3) allows us to approach the actual minimum $(z, \psi, \phi)_{\min}$ to within a sufficient level of precision to justify further analysis. Note that the presence of metastable minima in the free energy of adsorption is not taken into consideration by analysing the lowest free-energy value only.

Results of our Theoretical Study

An advantage of our model is that the r_{it} and r_{12} only have to be determined only once for a given q in order to establish $f(z, \psi, \phi)$ for different values of θ_i. To probe the effect of different surface patterning on $(z, \psi, \phi)_{\min}$, or equivalently different ligand concentrations on the facets, we varied $\cos\theta_i \in [-1, 1]$ in equidistant steps of 0.03.

Figure 3 shows the distribution of $(z, \psi, \phi)_{\min}$ in the 3D (z, ψ, ϕ) landscape upon varying the contact angles for $q = 0.30$. Note that the distribution of $(z, \psi, \phi)_{\min}$ is not homogeneous. In fact, an analysis of our results shows that the equilibrium orientations of the truncated cube can be roughly divided into three categories: (i) the normal of one of the {100} facets is pointing in the direction of the z-axis, (ii) the normal of one of the {110} facets is pointing in the direction of the z-axis, and (iii) the normal of one of the {111} facets is pointing in the direction of the z-axis, also see Fig. 4. We refer to these three configurations as the 'prototypical' configurations. This rough division assumes

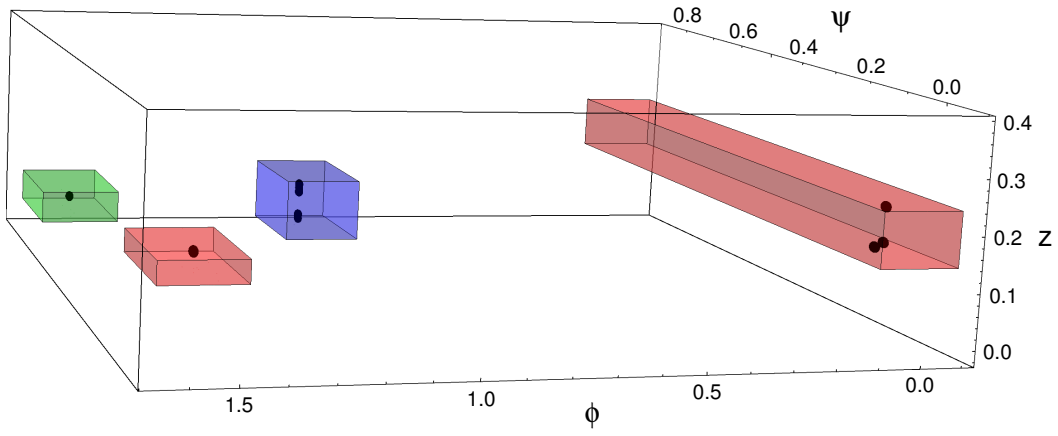

FIG. 3. The distribution of equilibrium adsorption configurations $(z, \psi, \phi)_{\min}$ (black dots) obtained by varying $\cos\theta_i \in [-1, 1]$ ($i = 1, 2, 3$) in equidistant steps of 0.03 for a truncated cube with $q = 0.30$. Note that the distribution of $(z, \psi, \phi)_{\min}$ is not homogeneous, only a few of the possible values of (z, ψ, ϕ) are assumed. The red, green, and blue translucent boxes indicate to which 'prototypical' configuration we assign these $(z, \psi, \phi)_{\min}$ points. Configurations in the red boxes correspond to adsorption with the normal of one of the {100} facets pointing in the direction of the z-axis, configurations in the green box correspond to adsorption with the normal of one of the {110} facets pointing in the direction of the z-axis, and configurations in the blue box correspond to the normal of one of the {111} facets pointing in the direction of the z-axis; also see Fig. 4, which uses the same colour coding. The two red boxes accommodate a single congruence class.

that, for instance, the state where the particle is adsorbed at depth z is equivalent to the one where it is adsorbed at depth $-z$. Moreover, we assume that $|\psi' - \psi| < 0.03\pi$ and $|\phi' - \phi| < 0.03\pi$ constitute the same configuration, where ψ' and ϕ' are the angles corresponding to the prototypical orientation of one of the three categories. The tolerance in the depth z is considered on a case-by-case basis.

Working backwards we can now find the three values of $\cos\theta_i$ for which the truncated cube is in one of the prototypical equilibrium configurations, see Fig. 4, which shows this correspondence. Here we only give $\cos\theta_1$, $\cos\theta_2 \in [-1, 1]$ and $\cos\theta_3 \in [0, 1]$, since the graph is point symmetric in the origin, which can be easily shown by considering the signs of the cos terms in Eq. (7). We find that the {100}-prototypical equilibrium configuration is the most common and there is a slightly greater number of {111} than {110} equilibrium configurations. However, it should be noted that interpreting the graph on the basis of surface area alone can be misleading, since $\theta_i \gtrsim 150^\circ$ and $\theta_i \lesssim 30^\circ$ represent atypical values of the contact values, i.e., $|\cos\theta| \lesssim 0.87$ is reasonable.

Following the approach that we employed for $q = 0.30$, we can study the influence of the surface properties of the different types of facet as a function of the level of truncation q, also see Figs. 5 - 8. Note that for $q = 0$ there are only two types of equilibrium configuration, one where one of the {100} facets is pointing upward, and one where one of the '{110} facets' is pointing upward. The first can be explained by the particle minimizing its contact area with the unfavoured medium, whilst still excluding a piece of the interface (thereby lowering its free energy). The second arises when there is a limited difference between the two media; the colloid can lower the free energy by excluding the maximum amount of surface area from the interface. N.B., for a cube ($q = 0$) the two prototypical configurations are the *only* two possible configurations within the confines of our model, i.e., there is no spread in the $(z, \psi, \phi)_{\min}$.

For small levels of truncation $q = 0.15$, see Fig. 6, the division into two prototypical equilibrium configurations ({100} and {110}) remains. The spread of the $(z, \psi, \phi)_{\min}$ around these configurations increases. The surface properties of the {110} facets have a small influence on the configurations that are assumed by the truncated cubes, as can be seen in Fig. 6. However, the presence of {111} facets do not seem to affect the equilibrium configurations sufficiently to cause the third prototypical configuration to appear.

Further truncation of the cube, see Fig. 4 for the $q = 0.30$ and Fig. 7 for the $q = 0.45$ result, respectively, appears to promote the {111} prototypical configuration. It is likely that a greater level of truncation destabilizes the the {110} configuration in favour of the {111} configuration, because the maximum amount of surface area that can be excluded from the interface in either configuration becomes comparable. This hypothesis was confirmed by considering truncated cubes with homogeneous surface properties, as well as other ways of truncating a cube [5].

However, when the level of truncation is great, see Fig. 8 for the $q = 0.60$ result, the truncated cube becomes rather spherical. This implies that there is no longer a limited number of favoured orientations on the basis of excluded

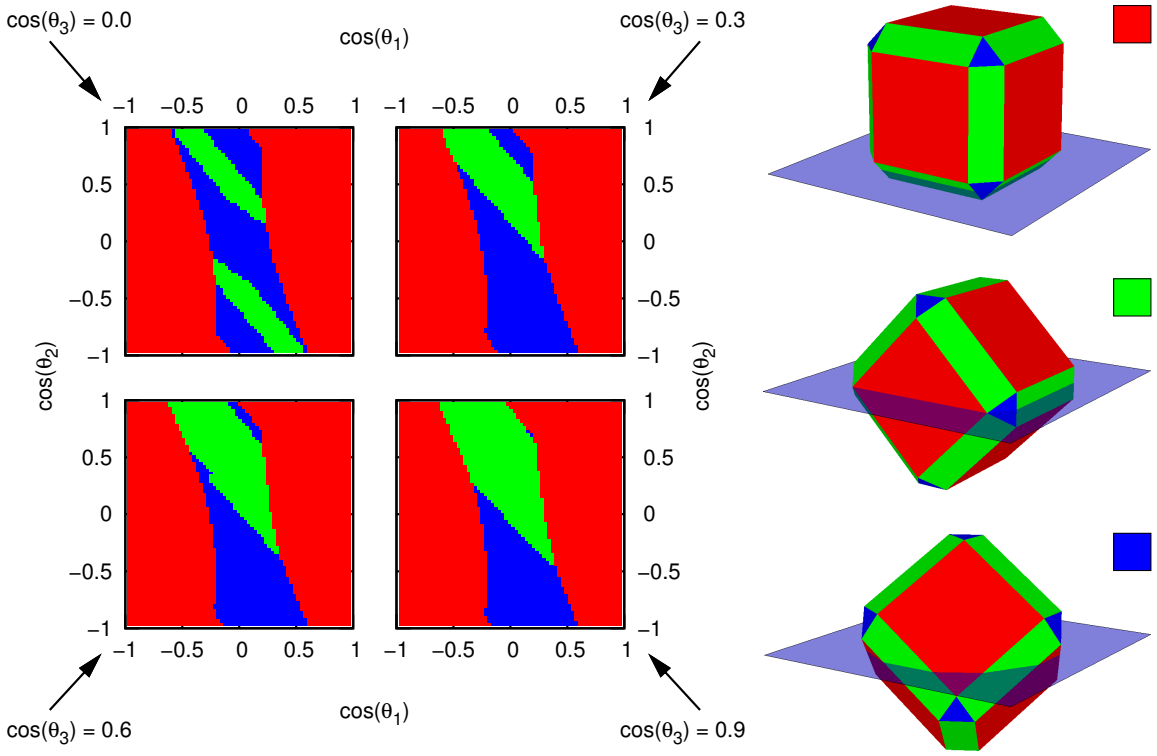

FIG. 4. The equilibrium configurations that present themselves for a truncated cube with truncation level $q = 0.30$ as a function of its surface properties. The sub-plots show four $\cos\theta_3$ slices: top, $\cos\theta_3 = 0.0$ (left) and $\cos\theta_3 = 0.3$ (right); bottom, $\cos\theta_3 = 0.6$ (left) and $\cos\theta_3 = 0.9$ (right). These indicate the prototypical equilibrium configuration that is assumed by the truncated cube as a function of $\cos\theta_1$ and $\cos\theta_2$. (legend) The three equilibrium configurations and associated colour code: (red) the normal of one of the {100} facets is pointing in the direction of the z-axis, (green) the normal of one of the {110} facets is pointing in the direction of the z-axis, and (blue) the normal of one of the {111} facets is pointing in the direction of the z-axis.

surface area arguments. As can be appreciated from Fig. 8 this results in a more coarse distribution of 'prototypical' equilibrium configurations, as well as the appearance of three more configurations.

Discussion and Outlook

Let us first consider the likelihood of interfacial adsorption. For a spherical particle with homogeneous surface properties the minimum difference in free energy ΔF between the adsorbed and desorbed state is easily shown to be given by $\Delta F = \pi a^2 \gamma_{12}(1 - |\cos\theta|)^2$. Here, a is the radius of the sphere, θ is the (air/liquid)-sphere-liquid contact angle, and γ_{12} is the interfacial surface tension. We can use this value to estimate what the strength of adsorption for our nanocrystals might be.

We assume that the nanocrystals are at the air/toluene interface, based on previous experimental observations for similar systems [6, 7]. The surface tension of the air/toluene interface is given by $\gamma_{12} \approx 2.8 \cdot 10^{-2}$ Nm^{-1} [8]. Note that finite values of $\cos\theta$ lower ΔF. However, for realistic values of θ this reduction in ΔF is no more than a factor of 10, with the maximum in ΔF assumed when $\cos\theta = 0$. The smaller nanocrystals, which have a diameter of 5.4 nm, therefore adsorb to the interface with at most $\Delta F \approx 1 \cdot 10^2$ $k_B T$, where k_B is Boltzmann's constant and T is the temperature. The larger nanocrystals, which have diameter of 9.9 nm, adsorb with at most $\Delta F \approx 5 \cdot 10^2$ $k_B T$. This *simple* estimate gives some ab initio justification of the applicability of our theoretical results to the experimental system. Under ideal circumstances there will be a strong influence of the interface on the nanoparticles, which drives these towards their equilibrium adsorption configuration. It should, however, be mentioned that these estimates do not factor into account surface-tension lowering effects such as the presence of surfactants at the interface or pollutants in the toluene.

Our results indicate that the three experimentally observed configurations can be explained within the framework of

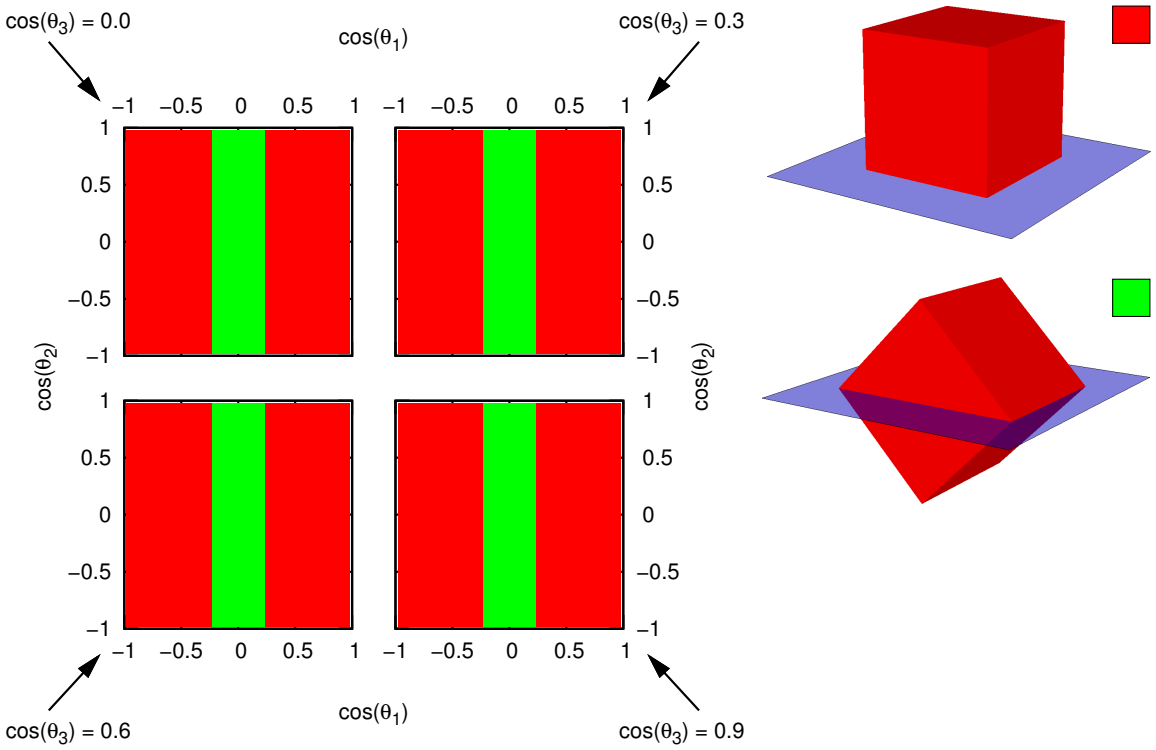

FIG. 5. The equilibrium configurations that present themselves for a cube ($q = 0$) as a function of its surface properties. The sub-plots indicate the (prototypical) equilibrium configuration that is assumed by the cube as a function of $\cos\theta_1$ and $\cos\theta_2$, for various $\cos\theta_3$ values. (legend) The two equilibrium configurations and associated colour code. Note that the type of configuration only depends on the surface properties of the red {100} facets, as expected for this level of truncation.

adsorption-desorption equilibria for the ligand concentration on the various facets. Indeed, upon varying the surface properties of the three types of facet - by modifying the contact angle - we theoretically found the possible equilibrium adsorption configurations to coincide with the orientations of the particles in the superstructures that formed at the interface. Moreover, it was experimentally observed that the level of truncation for the larger nanocrystals (9.9 nm) was less than that for the smaller variety (5.4 nm). This could explain the fact that the honeycomb structures were only observed for the smaller nanocrystals, since the {111} adsorption configuration does not occur for smaller levels of truncation, within the confines of our model.

We therefore propose the following explanation for our observations. At low concentrations of the truncated cubes the adsorption-desorption equilibrium for the ligands covering the facets is shifted towards the ligands being preferentially adsorbed in the ethylene glycol. When the truncated particles come together there is irreversible and disordered aggregation. However, for higher particle concentrations the equilibrium shifts to a sufficiently high ligand covering of the facets that immediate aggregation is prevented. Moreover, we believe that for these systems the surface properties of the nanoparticles are such that the equilibrium adsorption configuration is of the {100} or the {110} type, where the latter is preferentially assumed for lower particle concentrations. These configurations lead to the formation of two-dimensional (2D) rod-like ({110}) and square assemblies ({100}) by oriented attachment via the {100} facets, respectively. That is to say, for the {100}-like configuration, four of the {100} facets are oriented perpendicular to the interface, allowing for oriented attachment via these facets in the plane of the interface, which gives rise to square structures. For the {110} configuration, only two (opposing) {100} facets are perpendicular to the interface, allowing for oriented attachment that results in linear structures. Upon increasing the nanoparticle concentration from low to intermediate values, the ligand adsorption/desorption equilibria are shifted resulting in a different nanoparticle surface pattern. This surface pattern leads to preferential adsorption at the interface of the {111} type and subsequent oriented attachment via the (now) exposed {110} facets of the particles into honey-comb superstructures. The latter situation does not, however, occur when the level of truncation is too small to allow for the {111} configuration to be stable.

It is important to note that our results (and the conclusions we based on these) were obtained using a *simple* model

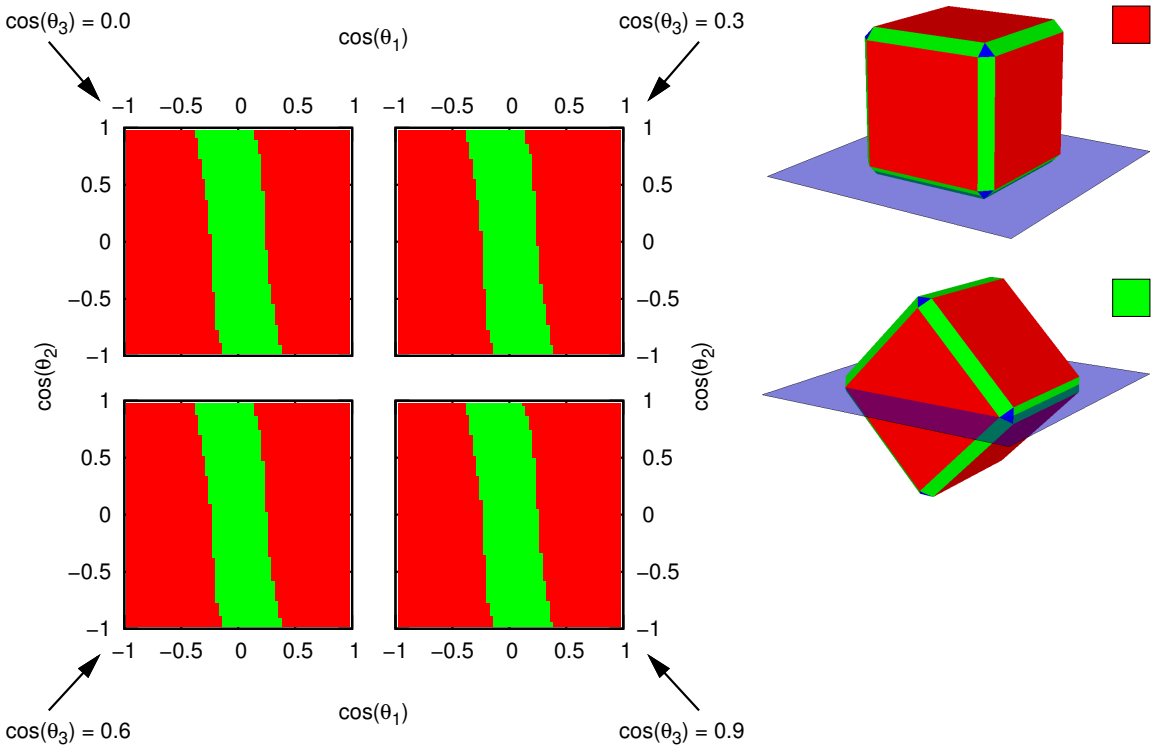

FIG. 6. The equilibrium configurations that present themselves for a truncated cube with truncation level $q = 0.15$ as a function of its surface properties. The sub-plots indicate the (prototypical) equilibrium configuration that is assumed by the truncated cube as a function of $\cos\theta_1$ and $\cos\theta_2$, for various $\cos\theta_3$ values. (legend) The two equilibrium configurations and associated colour code. Note that there is a small dependence on the surface properties of the {110} facets ($\cos\theta_2$) for this level of truncation. However, the surface properties of the {111} facets do not appear to play a role.

for the adsorption of a particle at a liquid-liquid or liquid-air interface. We leave a full investigation of the experimental phenomenology by theoretical or simulation means as an open problem for future study. An interesting question for such a study to answer is if a simple model that incorporates particle-concentration-based ligand adsorption-desorption equilibria, is capable of capturing the shift from the {100} towards the {111} equilibrium configuration, whilst at the same time showing a lower ligand covering of the facets which we believe to mediate the oriented attachment. A conformation of this shift would give strong support for our hypothesis that the interface and ligand adsorption/desorption play a crucial role in determining the structure of the assemblies that we observed to form by oriented attachment.

* D.vanmaekelbergh@uu.nl

[1] P. Pieranski, Phys. Rev. Lett. **45**, 569 (1980).
[2] T. Young, Phil. Trans. R. Soc. Lond. **95**, 65 (1805).
[3] J. de Graaf, M. Dijkstra, and R. van Roij, Phys. Rev. E **80**, 051405 (2009).
[4] J. de Graaf, M. Dijkstra, and R. van Roij, J. Chem. Phys. **132**, 164902 (2010).
[5] J. de Graaf, *Anisotropic nanocolloids: Self-Assembly, Interfacial Adsorption, and Electrostatic Screening*, PhD thesis, Utrecht University, 2012, ISBN 978-90-393-5797-2.
[6] H. Friedrich et al., Nano Lett. **9**, 2719 (2009).
[7] D. K. Smith, B. Goodfellow, D.-M. Smilgies, and B. A. Korgel, J. Am. Chem. Soc. **131**, 3281 (2009).
[8] A. W. Adamson and A. P. Gast, *Physical Chemistry of Surfaces*, Wiley-Interscience (New York), 6th edition, 1997.

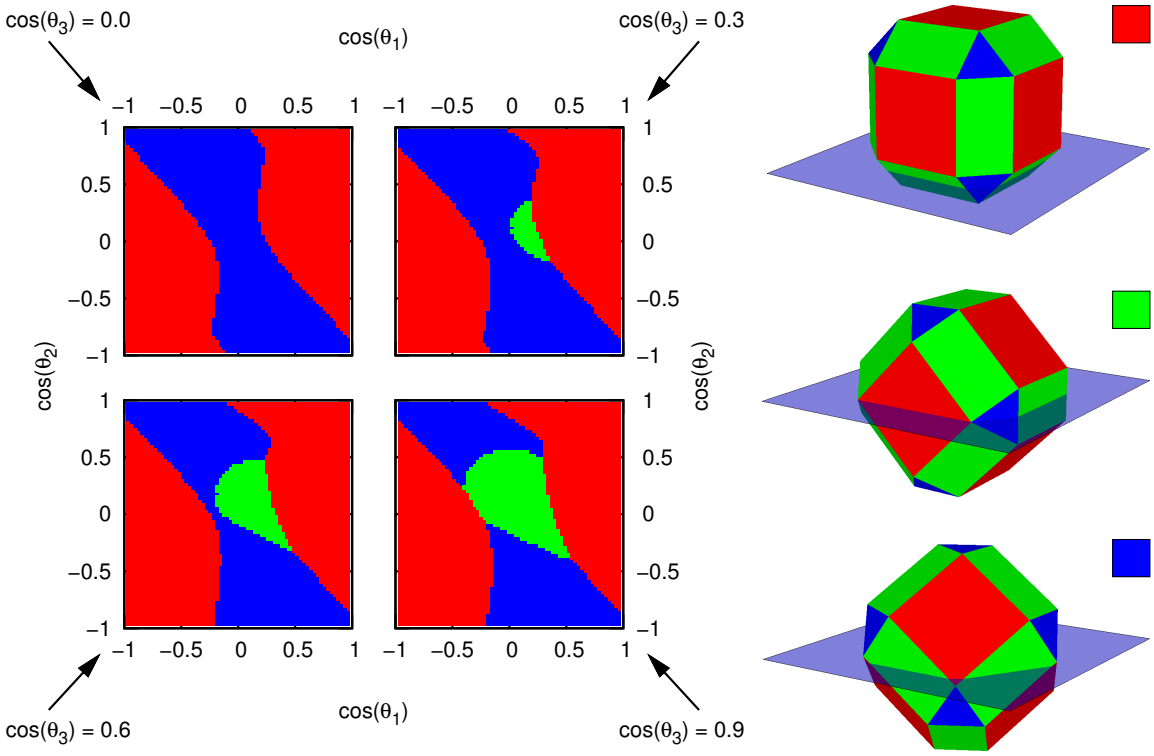

FIG. 7. The equilibrium configurations that present themselves for a truncated cube with truncation level $q = 0.45$ as a function of its surface properties. The sub-plots indicate the prototypical equilibrium configuration that is assumed by the truncated cube as a function of $\cos\theta_1$ and $\cos\theta_2$, for various $\cos\theta_3$ values. (legend) The three equilibrium configurations and associated colour code.

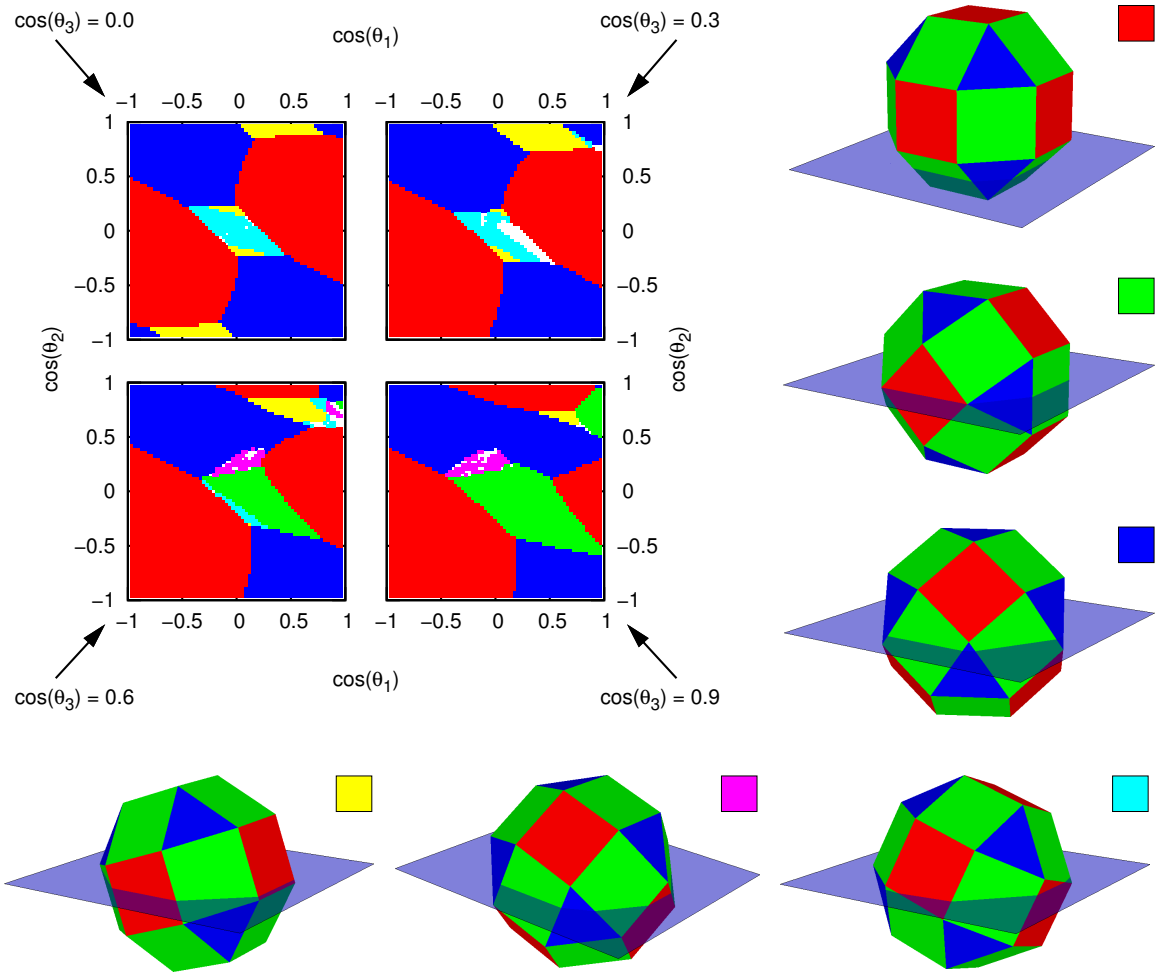

FIG. 8. The equilibrium configurations that present themselves for a truncated cube with truncation level $q = 0.60$ as a function of its surface properties. The sub-plots indicate the prototypical equilibrium configuration that is assumed by the truncated cube as a function of $\cos\theta_1$ and $\cos\theta_2$, for various $\cos\theta_3$ values. (legend) The six prototypical equilibrium configurations and associated colour codes. (red) one of the {100} facets is pointing in the direction of the z-axis, (green) one of the {110} facets is pointing in the direction of the z-axis, (blue) one of the {111} facets is pointing in the direction of the z-axis, (yellow) the {210} 'facet' is pointing in the direction of the z-axis, (magenta) the {221} 'facet' is pointing in the direction of the z-axis, and (cyan) the {321} 'facet' is pointing in the direction of the z-axis. The white points in the sub-plots indicate for which $\cos\theta_i$ combinations we were unable to assign a prototypical equilibrium configuration.